RESEARCH ARTICLE

Human Mutation

OFFICIAL JOURNAL
HGVS
HUMAN GENOME VARIATION SOCIETY
www.hgvs.org

Combined NGS Approaches Identify Mutations in the Intraflagellar Transport Gene *IFT140* in Skeletal Ciliopathies with Early Progressive Kidney Disease

Miriam Schmidts,[1] Valeska Frank,[2] Tobias Eisenberger,[2] Saeed al Turki,[3] Albane A. Bizet,[4,5] Dinu Antony,[1] Suzanne Rix,[1] Christian Decker,[2] Nadine Bachmann,[2] Martin Bald,[6] Tobias Vinke,[7] Burkhard Toenshoff,[7] Natalia Di Donato,[8] Theresa Neuhann,[8] Jane L. Hartley,[9] Eamonn R. Maher,[10] Radovan Bogdanović,[11,12] Amira Peco-Antić,[13] Christoph Mache,[14] Matthew E. Hurles,[3] Ivana Joksić,[15] Marija Guć-Šćekić,[11,16] Jelena Dobricic,[17] Mirjana Brankovic-Magic,[17] UK10K,[18] Hanno J. Bolz,[2,19] Gregory J. Pazour,[20] Philip L. Beales,[1] Peter J. Scambler,[1] Sophie Saunier,[4,5] Hannah M. Mitchison,[1]* and Carsten Bergmann[2,21]

[1]Molecular Medicine Unit, University College London (UCL) Institute of Child Health, London, UK; [2]Center for Human Genetics, Bioscientia, Ingelheim, Germany; [3]The Wellcome Trust Sanger Institute, Wellcome Trust Genome Campus, Hinxton, Cambridge, UK; [4]INSERM, U983, Hôpital Necker-Enfants Malades, Paris, France; [5]Université Paris Descartes-Sorbonne Paris Cité, Institut Imagine, Paris, France; [6]Department of Pediatric Nephrology, Olgahospital, Klinikum Stuttgart, Germany; [7]Department of Pediatrics, University Children's Hospital Heidelberg, Germany; [8]Institute of Human Genetics, Dresden University, Germany; [9]Liver Unit, Birmingham Children's Hospital, Birmingham, UK; [10]Department of Medical and Molecular Genetics and Centre for Rare Diseases and Personalised Medicine, University of Birmingham School of Medicine, Birmingham, UK; [11]Department of Nephrology, Institute of Mother and Child Health Care of Serbia "Dr Vukan, Čupić", Belgrade, Serbia; [12]Faculty of Medicine, University of Belgrade, Belgrade, Serbia; [13]Department of Nephrology, University Children's Hospital, Belgrade, Serbia; [14]Department of Pediatrics, Medical University Graz, Graz, Austria; [15] Clinic for Gynecology and Obstetrics, University Hospital, Belgrade, Serbia; [16]Faculty of Biology, University of Belgrade, Belgrade, Serbia; [17]Institute for Oncology and Radiology of Serbia, Belgrade, Serbia; [18]http://www.uk10k.org; [19]Department of Human Genetics, University of Cologne, Cologne, Germany; [20]Program in Molecular Medicine, University of Massachusetts Medical School, Worcester, Massachusetts; [21]Center for Clinical Research, University Hospital Freiburg, Freiburg, Germany

Communicated by Arnold Munnich

Received 5 July 2012; accepted revised manuscript 5 February 2013.
Published online 15 February 2013 in Wiley Online Library (www.wiley.com/humanmutation). DOI: 10.1002/humu.22294

ABSTRACT: Ciliopathies are genetically heterogeneous disorders characterized by variable expressivity and overlaps between different disease entities. This is exemplified by the short rib-polydactyly syndromes, Jeune, Sensenbrenner, and Mainzer-Saldino chondrodysplasia syndromes. These three syndromes are frequently caused by mutations in intraflagellar transport (IFT) genes affecting the primary cilia, which play a crucial role in skeletal and chondral development. Here, we identified mutations in *IFT140*, an IFT complex A gene, in five Jeune asphyxiating thoracic dystrophy (JATD) and two Mainzer-Saldino syndrome (MSS) families, by screening a cohort of 66 JATD/MSS patients using whole exome sequencing and targeted resequencing of a customized ciliopathy gene panel. We also found an enrichment of rare *IFT140* alleles in JATD compared with nonciliopathy diseases, implying putative modifier effects for certain alleles. *IFT140* patients presented with mild chest narrowing, but all had end-stage renal failure under 13 years of age and retinal dystrophy when examined for ocular dysfunction. This is consistent with the severe cystic phenotype of *Ift140* conditional knockout mice, and the higher level of *Ift140* expression in kidney and retina compared with the skeleton at E15.5 in the mouse. *IFT140* is therefore a major cause of cono-renal syndromes (JATD and MSS). The present study strengthens the rationale for *IFT140* screening in skeletal ciliopathy spectrum patients that have kidney disease and/or retinal dystrophy.
Hum Mutat 34:714–724, 2013. © 2013 Wiley Periodicals, Inc.

KEY WORDS: cilia; Jeune asphyxiating thoracic dystrophy; Mainzer-Saldino syndrome; IFT140; NGS

Introduction

An emerging number of diseases have been connected to the dysfunction of primary cilia and these disorders are now collectively termed "ciliopathies" [Baker and Beales, 2009]. Mutations in at least 50 genes have been identified in ciliopathies affecting sensory cilia functions [Baker and Beales, 2009]. A broad range of phenotypes affecting multiple organ systems are associated with defects in

Additional Supporting Information may be found in the online version of this article.

*Correspondence to: Hannah M. Mitchison, Molecular Medicine Unit, University College London (UCL) Institute of Child Health, London, UK. E-mail: h.mitchison@ucl.ac.uk

Contract grant sponsors: Wellcome Trust (WT091310) (UK10K); National Institutes of Health (GM060992) (GJP); Wellcome Trust Senior Research Fellow (PLB); Wellcome Trust and British Heart Foundation (PJS); Agence Nationale de la Recherchet (R09087KS and RPV11012KK) (SS); Deutsche Forschungsgemeinschaft (DFG BE 3910/4–1, DFG ZE 205/14–1, and SFB/TRR57) and Deutsche Nierenstiftung and PKD Foundation (CB); Action Medical Research UK and Henry Smith Charity SP4534, and Newlife Foundation for Disabled Children UK 10-11/15 (HMM); Action Medical Research UK Clinical Training Fellowship RTF-1411 (MS).

ciliary function and structure, which can be explained by their almost ubiquitous presence. Mammalian cilia have an axoneme composed of nine microtubule doublets derived from the centriole, or basal body within the centrosome. The cilium–centrosome complex has been conserved throughout evolution and across organ systems [Nigg and Raff, 2009]. Primary cilia operate as cellular signaling centers that detect and orchestrate various extracellular stimuli through specific ciliary receptors, and they are essential for fundamental cell signaling pathways that are required for embryonic development [Goetz and Anderson, 2010].

In view of the various skeletal phenotypes in ciliopathies, it is not surprising that primary cilia play a crucial role in skeletal and chondral development. Clinical overlap between different short rib-polydactyly syndromes and other osteochondrodysplasias clearly support allelism between some of these ciliopathies as part of a larger disease spectrum, for example, between Jeune, short rib-polydactyly type III, and Sensenbrenner syndromes, which share mutations in the same genes [Bredrup et al., 2012; Dagoneau et al., 2009; Lehman et al., 2010; Merrill et al., 2009]. Intriguingly, digenic biallelic inheritance involving combinations of the genes associated with these different syndromes has also been proposed as a disease mechanism, for example, in a patient with short rib-polydactyly type II (Majewski) carrying double heterozygous mutations in *NEK1* and *DYNC2H1* [Thiel et al., 2011].

Jeune asphyxiating thoracic dystrophy (JATD; MIM #208500), one of the short rib-polydactyly syndromes, has a variable presentation but the hallmark of disease is shortened ribs and a narrow, bell-shaped chest, which restricts lung growth causing respiratory insufficiency and frequent asphyxia-related perinatal death. Other features that occur more variably are short long bones and polydactyly, in addition to irregular spurs ("trident" shaped) on the acetabular bone and metaphysis, and cone-shaped epiphyses. Diverse extraskeletal features on the ciliopathy spectrum can also manifest including progressive cystic nephropathy, retinal dystrophy, pancreatic cysts, liver disease, and cholestasis [Beales et al., 2007; Dagoneau et al., 2009; Merrill et al., 2009; Oberklaid et al., 1977]. Mainzer-Saldino syndrome (MSS; MIM #266920) has only very recently been described as a cilia-related disease [Perrault et al., 2012], and like JATD it is counted as one of the "conorenal syndromes" due to impaired renal function and characteristic radiological findings of cone-shaped epiphyses. MSS may variously present with retinal dystrophy like JATD, and cerebral ataxia [Giedion, 1979; Mainzer et al., 1970; Mortellaro et al., 2010].

So far, five genes causing JATD have been reported, all encoding proteins involved in intraflagellar transport (IFT): *DYNC2H1* [Dagoneau et al., 2009; Merrill et al., 2009], *IFT80/WDR56* [Beales et al., 2007], *IFT139/TTC21B* [Davis et al., 2011], *IFT144/WDR19* [Bredrup et al., 2012], and most recently *IFT140* (MIM #614620) in one case of JATD [Perrault et al., 2012]. IFT is a complex, highly conserved process essential for ciliary formation, maintenance, and signaling functions whereby proteins synthesized and assembled in the cell body are transported along microtubules into (anterograde IFT) and out of (retrograde IFT) the cilium driven by kinesin and dynein motor proteins [Ishikawa and Marshall, 2011]. Dysfunctional IFT in mouse JATD models affects targeting of the hedgehog receptor smoothened to the cilium [Ocbina and Anderson, 2008; Rix et al., 2011], explaining the phenotypic similarities observed between IFT mutants and mice carrying mutations in genes directly influencing hedgehog signaling [Huangfu and Anderson, 2005].

Although we previously reported some evidence that *IFT80* patients present with milder disease and no extraskeletal findings [Beales et al., 2007], overall no convincing genotype–phenotype correlations have been claimed for patients with JATD and related disorders carrying mutations in different components of the IFT machinery. While cystic kidney disease is a well-accepted feature in JATD [Donaldson et al., 1985; Oberklaid et al., 1977], in fact only two patients in the literature with mutations in defined JATD genes have kidney symptoms; one with *IFT144* mutations, one with *IFT140* mutations [Bedrup et al., 2012; Perrault et al., 2012]. Thus, the molecular basis of the variable kidney symptoms seen in JATD is not yet well understood.

In this study, we present the results of gene identification efforts initiated using a large JATD cohort that combined next-generation sequencing (NGS) approaches of whole exome sequencing (WES) and targeting of a 131 ciliopathy gene panel. Subsequent follow up focused on *IFT140* in additional JATD and MSS families, in order to investigate the correlation between the phenotype and underlying genotype in these genetically heterogeneous conditions, as well as the potential disease modifying effects of heterozygous *IFT140* variants.

Materials and Methods

Patient and Control Samples and Genomic DNA Extraction

All patient samples in this study were obtained with informed consent according to the protocols approved by the ethical committees of the Institute of Child Health/Great Ormond Street Hospital and University College London Hospital NHS Trust, and those of collaborating institutions.

Inclusion criteria for WES and ciliopathy gene panel NGS sequencing was clinical diagnosis of JATD or MSS and a sufficient DNA amount. Inclusion criteria for Sanger sequencing of *IFT140* was clinical diagnosis of JATD with renal disease. Serbian samples from individuals unaffected by ciliopathy disorders were provided from the Institute for Oncology and Radiology of Serbia.

Whole Exome Sequencing

DNA (1–3 μg) sheared to 100–400 bp (Covaris, Woburn, MA) was used for Illumina paired-end DNA library preparation and enriched for target sequences (Agilent Technologies Inc, Loveland, Colorado, USA; Human All Exon 50 Mb kit). Enriched libraries were sequenced as 75 base-paired-end reads (Illumina HiSeq, Illumina Inc. San Diego, California, USA). Sequencing reads that failed quality filtering were removed using the Illumina GA Pipeline and passed reads mapped to human genome reference hg19 using BWA v0.5.9r16 [Li and Durbin, 2010]. GATK 1.1.5 [McKenna et al., 2010] was used to realign around known indels from the 1000 Genomes Pilot and recalibrate base quality scores. Variants were called and filtered independently with SAMtools mpileup v0.1.17 [Li et al., 2009] and GATK UnifiedGenotyper v1.3.31 [DePristo et al., 2011] and the callsets merged. Exome variant profiles were filtered using EVAR software tool versus 0.2.2 beta (www.exome.info), for novelty and minor allele frequency (MAF) < 0.005, then filtered by quality score using a standard cut-off value that implicates a base error rate <0.1%. Synonymous coding variants, and those not conferring missense, nonsense, frameshift, and splice site mutational effects in coding regions were removed, then any variants present in 500 control exomes available via the UK10K project with an allele frequency >0.5% were removed. Finally, a screen for homology to genes present in the cilia proteome was performed [Gherman et al., 2006].

NGS Ciliopathies Panel Analysis

DNA was enriched using NimbleGen SeqCap EZ choice sequence capture and 454 GS FLX pyrosequencing according to the manufacturer´s protocol. Five hundred nanograms of genomic DNA were fragmented (Covaris S2 AFA) and ligated to barcoded adaptors for multiplexing. Precapture amplified samples were pooled and hybridized to the customized in-solution capture library, subsequently eluted and postcapture amplified by ligation mediated PCR. This amplified enriched DNA was used as input for emulsion PCR and subsequent massive parallel sequencing on one full picotiter plate of a Roche 454 GS FLX platform. Bioinformatic analysis was performed using the Roche GS Reference Mapper^{TM} software (v2.6), SeqPilot SeqNext module^{TM} (v3.5.2; JSI medical systems, Kippenheim, Germany) as well as an in-house bioinformatic pipeline. Information on genes other than *IFT140* sequenced on this panel is available on request.

Sanger Sequencing

Primers for *IFT140* coding exons and flanking intron–exon boundaries are available on request and were designed using PrimerBlast (http://www.ncbi.nlm.nih.gov/tools/primer-blast/). PCR reactions (Biotaq PCR kit; Gentaur Ltd. London, UK) were purified using Microclean. Sequencing was performed at SourceBioscience, UK or Bioscientia, Germany (ABI 3500xL genetic analyzer; Applied Biosystems, Life Technologies, Carlsbad, California, USA). Sequences were analyzed using the Sequencher program and commercial JSI software. Mutation annotation was performed on *IFT140* NM_014714.3.

Mutation Nomenclature

Mutation nomenclature follows the HGVS guidelines (http://www.hgvs.org/mutnomen/), and mutations throughout are referred to by either their cDNA numbering with +1 corresponding to the A of the ATG translation initiation codon; or using amino acid nomenclature, where the initiation codon is codon 1. Mutation information has been submitted to the LOVD database: www.lovd.nl/IFT140.

IFT140 Variant Enrichment Analysis

Files on 46 JATD, 71 hypercholesterolemia, 63 severe insulin resistance patients available through the UK10K project were processed using the same pipeline. Effects on protein function were predicted using PolyPhen-2 [Adzhubei et al., 2010]. Statistical analysis was performed using Fisher's Exact Test.

IFT140 Immunofluorescence

Murine ATDC5 chondrocytes were cultured (DMEM-F12, 10% FBS; Invitrogen, Life Technologies, Carlsbad, California, USA) until confluent then serum starved in 0.05% FBS for 72 hr. The cells were then washed in PBS, fixed with 4% paraformaldehyde for 10 min at room temperature, washed five times with PBS and permeabilized with 0.05% TritonX100 for 10 min. After five more washes with PBS cells were incubated with 5% bovine serum albumin (Invitrogen) in PBS then incubated with anti-IFT140 rabbit polyclonal antibody 1:500 [Jonassen et al., 2012] and monoclonal mouse antiacetylated tubulin 1:1,000 (Sigma, St Louis, Missouri, USA) overnight at 4°C. After five washes with PBS cells were incubated with secondary antirabbit antibody (Alexa Fluor 488 goat antirabbit IgG; Invitrogen) and secondary antimouse antibody (Alexa Fluor 594 donkey antimouse IgG; Invitrogen). Cells were finally washed five times with PBS, coverslips mounted in AF1 (Citifluor Ltd., Leicester, UK), and imaged using a Zeiss Axio Imager Z1 microscope.

Localization of IFT140 Mutants in RPE1

hTERT-RPE1 cells were cultured at 37°C, 7% CO_2 in D-MEM-F12 medium with 10% FBS, 2 mM L-glutamine and 1% streptomycin/penicillin (Invitrogen). Cells were seeded on glass coverslips (3×10^4 cells/well) and transfected using Fugene HD (Promega, Madison, Wisconsin, USA), according to the manufacturer's instructions, with 0.25 μg/well of the following plasmid DNA: pCMV-IFT140-WT-Flag [Perrault et al., 2012], pCMV-IFT140-V292M-Flag obtained by site directed mutagenesis, or pCMV-IFT140-E664K-Flag [Perrault et al., 2012]. At 48 hr posttransfection, cells were fixed with ice-cold methanol for 5 min and washed twice with PBS. Nonspecific sites were blocked with 10% goat serum (Sigma) and the cells were incubated with goat polyclonal anti-γ-tubulin (SC-7396, 1:200; Santa Cruz Biotechnology, Palo Alto, California, USA) and rabbit anti-Flag antibodies (1:400; Sigma–Aldrich, St Louis, Missouri, USA). After three washes, cells were incubated with secondary antibodies (AlexaFluor 488 conjugated antigoat, 1:200, and AlexaFluor 555 conjugated antirabbit antibodies, 1:200; Molecular Probes, Life Technologies, Carlsbad, California). Cells were then washed three times with PBS, incubated for 5 min with Hoechst and mounted in Fluo-prep. Confocal images were taken using a LEICA SP5 laser scanning microscope system with an ×63.2 objective (Carl Leica, Wetzlar, Germany). The percentage of transfected cells displaying localization of IFT140 at the centrosome was calculated from three independent experiments ($n > 100$ cells for each transfection condition). The significance of variations between mutants and wild-type-IFT140 was estimated using Dunnett's Multiple Comparison Test following the analysis of variance (ANOVA) test (GraphPad Prism software).

Ift140-lac*Z* Reporter Mouse and *X-Gal*-Staining

Ift140 lac-Z reporter mice were generated using the previously described *Ift140loxP* line generated by G.J.P [Jonassen et al., 2012]. *Ift140*-loxP heterozygous males were crossed with wild-type females and litters harvested at E15.5. Embryos were genotyped as previously described [Jonassen et al., 2012] and X-Gal staining was performed as previously described (Nagy et al., 2003). Briefly, embryos were fixed for 30 min in Beta-Gal fix (1% PFA, 0.2% glutaraldehyde) and stored in 30% sucrose overnight at 4°C. Embryos were then mounted in OCT and frozen at –80°C before being cryosectioned at 30 μm. Sections were incubated in X-Gal staining solution containing 5 mM K3Fe, 5 mM K4Fe, and 0.5 mg/ml X-gal at 37°C for 24 hr. Sections were lightly counterstained in aqueous eosin for 45 sec, washed in tap water for 10 min, and dry mounted in DPX (Merck Millipore, Darmstadt, Germany). Images were taken using an Axio Imager microscope from Zeiss, Jena, Germany.

Results

We initially performed WES to identify the underlying molecular basis of disease in 46 individuals with a clinical diagnosis of JATD. WES was performed at the Wellcome Trust Sanger Institute

Table 1. Skeletal Dysplasia Patients with Early Onset Renal Involvement Harboring *IFT140* Mutations

Patient	JATD1	JATD2	JATD3	JATD4	JATD5	MSS1	MSS2
Ethnic background	Serbian	Serbian	German	Serbian	Lithuanian	Austrian	German
Clinical diagnosis	JATD	JATD	JATD	JATD	JATD	MSS	MSS
Current age	12 years	17 years	3 years	24 years	na	39 years	5 years
Genotype	c.1380delC (p.N460Kfs28*) (Mat)/c.874C>T (p.V292M) (Pat)	c.1565G>A (p.G522E) (Pat)/c.874C>T (p.V292M) (Mat)	c.454C>T (p.L152F) (Mat)/c.454C>T (p.L152F) (Pat)	c.1565G>A (p.G522E) (Pat)/c.874C>T (p.V292M) (Mat)	c.2278C>T (p.R759*) (Pat)/?	c.2399+1G>T (Mat)/ c.4078T>C (p.C1360R) (Pat)	c.418G>A (p.G140R) (Mat)/c.800A>G (p.E267G) (Mat)/c.490G>T (p.E164*) (Pat)
Mutation analysis	WES	SS	TR panel	SS	SS	TR panel	TR panel
Respiratory insufficiency in early infancy	+	–	–	–	+	–	–
Brachymesophalangism	+	+	+	+	+	+	+
Short stature	P3–10	P50	P3–10	<P3	+	+ (<P3)	P10
Small thorax	+	+	+	+	+	+	+
Polydactyly	–	–	–	–	–	–	–
Cone-shaped epiphyses	+	+	+	+	+	+	+
Facial dysmorphism	Low set ears	–	Prominent forehead, high arched palate	–	–	Low set ears, prominent forehead	–
Vision	Retinal pigmentary dystrophy age 2 y (fundoscopy)	Hypermetropia, hyperpigmented retina age 17 y (fundoscopy)	Strabism, nystagm, hyperopia with astigmatism, night blindness age 4 y	Night blindness since age 2 y, retinal pigmentary dystrophy age 9 y (fundoscopy)	na	Retinal pigmentary dystrophy with childhood onset (fundoscopy), myopia, cataract	Night blindness, beginning retinal pigmentary dystrophy (fundoscopy), silent ERG age 6 y, hyperopia
Renal insufficiency	ESRF age 4 y	ESRF age 6 y	ESRF age 6 mths	ESRF age 7 y	ESRF age 7 mths	ESRF age 12 y	ESRF age 4 y
Renal ultrasound	Increased echogenicity, multiple cortical cysts	Increased echogenicity	Increased echogenicity, diminished corticomedullary differentiation	Increased echogenicity, diminished corticomedullary differentiation	na	Small hyperechogenic kidneys, cortical cysts	Enlarged kidneys with multiple cysts of different size, increased echogenicity, diminished corticomedullary differentiation
Arterial hypertension	+	–	+	–	na	+	+
Pancreatic cysts	–	–	–	–	–	–	–
Liver disease	–	–	Slightly enlarged liver with increased echogenicity	–	Enlarged liver	–	
Psychomotor development	Normal	Normal	Slightly retarded	Normal	na	Retarded	Normal
Other		Pectus carinatus	Mitral insufficiency 1°			Coxarthrosis	Secondary hyperparathyroidism

WES, whole exome sequencing; SS, Sanger candidate gene sequencing; TR panel, targeted resequencing ciliopathies panel; P, percentile; ESRF, end-stage renal failure; na, not available.

(Cambridge, UK) as part of the UK10K project (http://www.uk10k.org/), and the sequence coverage and quality analysis was equivalent for all 46 samples. A representative example for one affected individual, JATD1, is detailed in Supp. Table S1. Variants were filtered to exclude those inconsistent with autosomal recessive inheritance, then assessed for novelty, firstly using EVAR software to exclude any present in the 1000 Genomes database [2010] and NHLBI Exome Sequencing Project Exome Variant Server (EVS) (http//:evs.gs.washington.edu/EVS) with a MAF >0.005, a cut-off selected assuming a disease frequency of JATD <1:200,000. Variants were next filtered for quality score and in view of the JATD disease model, we then focused on nonsynonymous coding variants conferring missense, nonsense, frameshift, and splice site mutational effects. Finally, variants present in 500 control exomes available via the UK10K project with an allele frequency >0.5% were removed, and a screen for homology to genes present in the cilia proteome was performed.

This filtering process for the single affected patient from the Serbian-origin family JATD1, is shown in Supp. Table S2. After filtering, in JATD1 unique compound heterozygous changes in *ADAMTS18*, *CCDC51*, *KIAA1274*, and *IFT140* and unique homozygous changes in *ARHGAP23*, *ZNF541*, *ZNF714*, and *PCDHGB2* were identified. The final filter against the cilia proteome [Gherman et al., 2006] prioritized compound heterozygous mutations in two genes: *CCDC51*, a protein of unknown function (c.1181C>G, p.C394S, and c.11C>T. p.R4H, both predicted benign by Polyphen2 and SIFT) (Supp. Table S3); and *IFT140* (c.1380delC; p.N460Kfs28*, and c.874G>A; p.V292M) (Table 1, Supp. Table S4). Because of the presence of a nonsense allele and given its known role in IFT, we prioritized *IFT140* for further analysis. All the unique

biallelic variants in the seven genes identified in JATD1 apart from *IFT140* are listed in Supp. Table S3 for comparison, along with the putative gene function, to show why these candidates were excluded from further analysis based on their having nondeleterious changes or a gene function unconnected to cilia functions. None of the 45 JATD patients apart from JATD1 that were screened by WES carried two predicted mutant *IFT140* alleles, nor mutant alleles in any of the seven other genes highlighted in JATD1 (their full details are shown in Supp. Table S5).

The JATD1 patient was notable for having had severe kidney involvement requiring kidney transplant during childhood, as well as retinal disease, as detailed in Table 1. In addition, typical skeletal features of JATD were present in this patient (Fig. 1A, F, and L). We proceeded to screen additional patients using a diagnostic NGS panel developed for ciliopathies encompassing all exons and adjacent intronic boundaries of 131 known ciliopathy genes. This totaled 2,412 coding exons of genes selected from cilia proteome and ciliary trafficking studies (Frank et al., 2012). These comprised an additional 12 JATD cases and, in view of the potentially overlapping renal-skeletal disease spectrum, two MSS cases. This revealed an additional patient, JATD3, from a German family carrying an *IFT140* homozygous missense mutation (c.454C>T; p.L152F), who had early onset renal disease and onset of hemeralopia and night blindness at the age of 4 years; ERG has not been performed (Fig. 1I, N, and O). We also defined biallelic *IFT140* mutations in both MSS patients: MSS1 a patient of Austrian origin carried a missense change c.4078T>C; p.C1360R in combination with a predicted splice site mutation, c.2399+1G>T affecting the essential 100% conserved exon 19 splice donor site and predicting a protein frameshift and early termination (Table 1, Supp. Table S4). The latter variant has recently been identified in a JATD and another MSS case [Perrault et al., 2012]; MSS2 a patient of German origin with typical features (Fig. 1C–E, H, J, and K) carried three *IFT140* changes, a paternally inherited nonsense mutation c.490G>T; p.E164* as well as two maternally inherited variants, c.418G>A; p.G140R and c.800A>G; p.E267G (Table 1, Supp. Table S4).

We also screened *IFT140* in six additional JATD patients with skeletal phenotypes accompanied by significant renal disease, using Sanger sequencing of all 29 coding exons. This revealed two additional Serbian-origin JATD patients (JATD2, JATD4) both carrying compound heterozygous changes consisting of the p.V292M mutation originally identified in Serbian JATD1, in combination with a second missense change c.1565G>A; p.G522E (Table 1, Supp. Table S4). In addition, patient JATD5 from a Lithuanian origin family carried a single heterozygous *IFT140* nonsense mutation c.2278C>T; p.R759* (Table 1, Supp. Table S4); we cannot exclude that a second deleterious *IFT140* allele remains undetected in this patient, for example a copy number or promoter variation.

All the *IFT140* variants detailed in Table 1 were absent or had a MAF <0.5% in available control populations comprising the 1000 Genomes and EVS exome collections, dbNSFP v1.3 [Liu et al., 2011], dbSNP v135, and the HGMD® Professional 2011.4 database (9.12.11 release), as well as 500 control exomes available via the UK10K project. The p.G522E and p.V292M mutations that are shared in common between the three Serbian JATD patients JATD1, JATD2, and JATD4 (Table 1), were screened for in 110 Serbian control chromosomes and found to be absent. We suggest that these alleles most likely represent *IFT140* ancestral founder effect mutations, however we do not have haplotype evidence to support this hypothesis. All deleterious alleles were confirmed by Sanger sequencing in the patients, and sequencing of all the available family members confirmed an autosomal recessive inheritance in all cases indicating correct segregation of sequence variants with the disease (Table 1, Supp. Fig. S1). Because of a lack of RNA, we were unable to analyze the detected mutations at the RNA level to rule out the likelihood of a cryptic splicing event or similar defect.

Using five different bioinfomatic tools, Mutationtaster, Polyphen2, PMut, CONDEL and LRT [Adzhubei et al., 2010; Ferrer-Costa et al., 2005; Gonzalez-Perez and Lopez-Bigas, 2011; Liu et al., 2011; Schwarz et al., 2010], all these *IFT140* variants (bialleic and monoallelic) were scored overall as probably damaging and deleterious. The locations of the ten putative *IFT140* mutations we identified, listed in Table 1, are shown in the gene and corresponding protein structure in Figure 2A. The amino acids affected by the six missense mutations found are well conserved among species implying functional importance (Supp. Fig. S2), and occur early on toward the N-terminus of the protein except for C1360. The affected residues L152, E267, and G522 are the most highly conserved across species in our alignment, including *Caenorhabditis elegans*.

The p.V292M change shared in common between three Serbian patients JATD1, 2 and 4 scored as possibly damaging in Polyphen2 but neutral in PMut, whereas the homozygous change p.L152F was scored as neutral in Polyphen2 and neutral in PMut (Supp. Table S4). We therefore analyzed both changes further for their putative effect on IFT140 function using the SWISS-MODEL service via the ExPASy Web server (http://swissmodel.expasy.org/) to construct wild-type and mutated IFT140 protein models, which were further analyzed and visualized for changes of protein folding and structure by UCSF Chimera [Meng et al., 2006; Yang et al., 2011]. The quality of this protein modeling was judged reasonably high using I-TASSER [Roy et al., 2010] with a confidence score –0.83 (typical range is –5 to +2). V292M is located in the predicted WD-repeat 4 of IFT140 (Fig. 2A) at the edge of a beta-sheet folded protein region (Fig. 2B). The substitution of a methionine in place of the valine residue creates a more protruding, longer side chain, which might reduce the distance to neighboring residues therefore affecting protein configuration even though both side chains are hydrophobic. Additionally, it introduces a sulfur atom. Similarly for p.L152F, substitution of the phenylalanine in place of leucine potentially greatly disturbs the normal structure, in this case due to the large phenol ring probably distorted to point toward the outside of the protein, changing the protein configuration (Fig. 2B). Both mutations change van-der-Waals-forces at the residues where the mutations occur, as shown in Fig. 2B. The mutations modeled in the wider protein context are shown in Supp. Fig. S3.

In addition to the suggested effects on protein folding, insertion of different side chains might affect protein–protein interactions. As the p.V292M mutation directly affects WD4, a change in its configuration potentially disturbs formation of a WD domain which usually consists of 4–16 WD repeats assembled into a circular beta-propeller structure. WD domains occur in numerous different proteins and are highly conserved among species, functioning as scaffolds in protein-complex formation. Interestingly, the specificity of the WD domain seems to depend on sequences around the WD domain rather than the WD domain itself, therefore the L152D mutation could interfere with the specificity of the WD domain [Li and Roberts, 2001]. We proceeded to analyze the effect of the p.V292M mutation on protein stability and localization *in vivo* in RPE1 hTERT-immortalized retinal pigment epithelial cells that are commonly used for primary cilia cell biology studies. Although flag-tagged IFT140 localizes to centrosomes in the majority of cells examined, mutant protein carrying the p.V292M missense change was absent from centrosome in most cells (Fig. 3). The same effect was observed for mutant protein carrying a disease-causing IFT140 E664K mutation, as has also previously been reported using the same

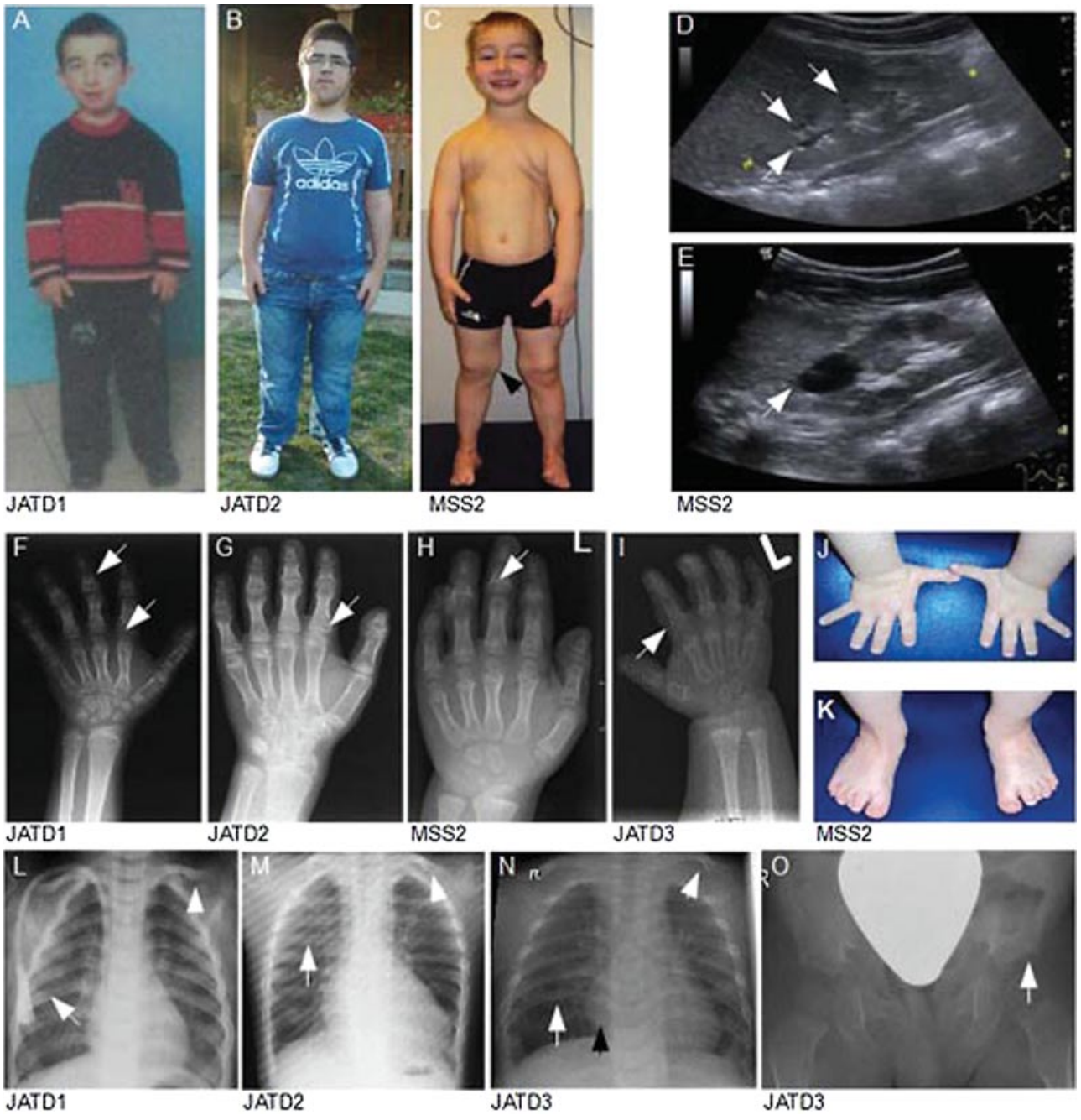

Figure 1. Phenotypes of affected individuals with *IFT140* mutations. Representative images of JATD and MSS patients with *IFT140* mutations. **A**–**C**: Patients in families JATD1, JATD2, and MSS2 exhibit dysproportionate short stature with short extremities and relatively narrow thoraces, note the distinct tibia epiphyses in MSS2 (black arrow). **D and E**: Renal ultrasound demonstrating increased echogeneity and cyst formation (arrows) in the MSS2 patient. **F**–**I**: Hand X-rays for patients JATD1, JATD2, JATD3, and MSS2 reveal cone-shaped epiphyses (arrows) and brachymesophalangism. **J and K**: Typical broad hands and feet with short fingers and broad short toes in MSS2. **L**–**N**: Thoracic X-rays taken at the age of 7 years in JATD1 (**L**) and in infancy in JATD2 and JATD3 (**M and N**) showing horizontal but only mildly to moderately shortened ribs with intermittent irregular rib shape (intermittent thickening) (**L**–**N**, white arrows on the left). Black arrowhead in (**N**) indicates typical widening of the costo-chondral junctions. Patients also show typical handlebar clavicle configuration (**L**–**N**, white arrowheads on the right). Arrow in (**O**) indicates mild acetabular spurring, a hallmark of JATD.

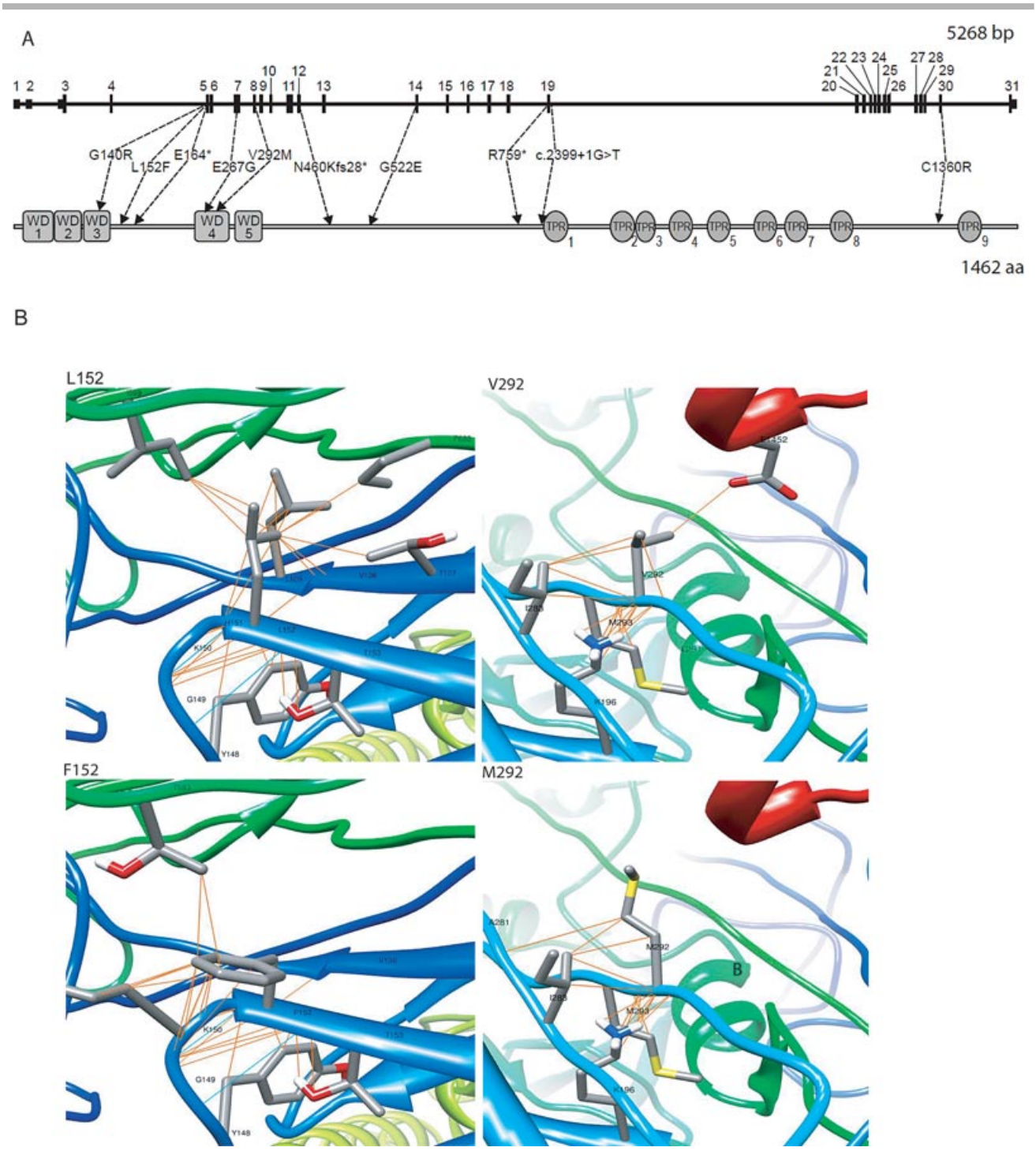

Figure 2. *IFT140* mutations and their impact on protein structure. **A**: The 31 exon *IFT140* gene (ATG located in exon 3) is shown (top panel) in relation to the protein domains. WD40 (WD) and tetratricopeptide (TPR) repeat containing domains are shown in boxes along the protein sequence. The locations of the identified variants in *IFT140* are indicated by the arrows. Note that only variants identified in biallelic patients are shown, apart from p.R759* identified in JATD5. **B**: The effects of missense mutations p.L152F and p.V292M on the IFT140 tertiary structure. The normal (top panels) and mutated (bottom panels) amino-acid sequences are illustrated, showing the effects of missense mutations L152F and V292M on hydrogen bonds (blue) and van-der-Waals-forces (orange) as detailed in the text.

system [Perrault et al., 2012]. The V292M-mediated mislocalization may potentially be due to abrogated protein–protein interactions.

Thus, in addition to the two MSS patients, we screened a total of 64 JATD patients by WES, NGS panel, and Sanger sequencing. The clinical details of the entire cohort are shown in Supp. Table S5. In total, we identified biallelic deleterious *IFT140* mutations in 4/64 JATD (6%) and 2/2 (100%) MSS families. Renal ultrasound revealed increased echogenicity in all these *IFT140* JATD and MSS patients, and three patients (JATD1, MSS1, and MSS2) had cystic kidney disease. Patients JATD1, JATD4, MSS1, and MSS2

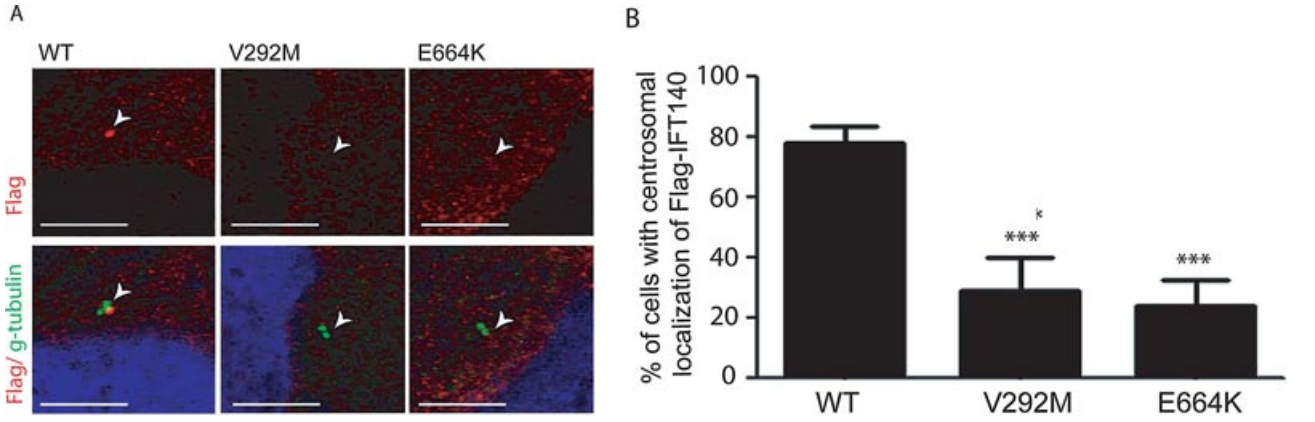

Figure 3. Mislocalization of Flag-tagged mutant IFT140 proteins in RPE1 cells. Centrosomes were stained with goat anti-γ-tubulin (green) IFT140 plasmids with rabbit anti-Flag (red), in cells transfected with pCMV-IFT140-WT-Flag, pCMV-IFT140-V292M-Flag or pCMV-IFT140-E664K-Flag plasmids. Scale bars, 6 μm. Wild-type (WT) IFT140 is clearly visible at the basal body (white arrow), whereas both V292M and E664K mutant proteins display decreased centrosomal labeling, as described previously for the E664K mutant [Perrault et al., 2012]. The graph shows the percentage of transfected cells with Flag-tagged IFT140 protein localized at the basal body, calculated from three independent experiments ($n > 100$ cells per transfection condition ($^{***}P < 0.001$ calculated using Dunn's Multiple Comparison Test following the analysis of variance [ANOVA] test (GraphPad Prism Software).

were diagnosed with retinal disease during childhood, whereas patient JATD3 had a normal fundoscopy result when aged 3 years but developed hemeralopia when aged 4 years. In patient JATD2, fundoscopy was normal during childhood but follow up screening at the age of 17 years revealed mild hyperpigmentation indicative of retinal disease. ERG was not performed in most patients, but was found to be silent in the MSS patients who were examined (example shown in Supp. Fig. S4). In total, signs of retinal disease were overt in four out of five *IFT140* patients, and one patient (JATD5) was lost to follow up, so the development of retinal disease in later life cannot be excluded, while retinal disease was observed in just seven of 64 patients of the total JATD cohort screened (11%). However, we did not detect *IFT140* mutations in three JATD families from this cohort who had retinal disease but normal renal function (JATD19, JATD20, JATD21, Supp. Table S5).

All the JATD patients, we found to carry deleterious *IFT140* mutations presented with cone-shaped epiphyses, brachymesophalangism, and small thoraces, but only two (JATD1 and JATD5) showed respiratory insufficiency and no patient was found to have polydactyly. All *IFT140* patients but patient JATD2 were of short stature (Table 1); this contrasts with the lack of significant height deficit seen in JATD patients that we have identified to carry disease-causing *DYNC2H1* mutations [Schmidts et al., 2013], and might well be secondary to renal insufficiency in *IFT140* patients.

In addition to the mutations described, WES also detected a further four patients JATD6, 7, 8, and 9 carrying a single unique heterozygous *IFT140* variant without a second allele being found (Supp. Table S4), who did not have renal or retinal disease. Of these heterozygous missense changes, p.P1353R, p.D787G, and p.L514H in JATD7, 8, and 9, respectively, are predicted in bioinformatics analysis to abrogate protein function, whereas JATD6 carried in heterozygous form the same c.2399+1C>A essential splice donor mutation as MSS1, and as previously reported by Perrault et al. (2012) (Supp. Table S4). We cannot say whether *IFT140* is the cause of their disease, but these monoallelic variants p.P1353R, p.D787G, and p.L514H all affect resiss well-conserved outside vertebrates (Supp. Fig. S2). It is possible such variants could modulate the *IFT140*-related skeletal dysfunction in patients when present in heterozygous state. Three heterozygous variants predicted to be benign were also identified in families JATD10–12 (Supp. Table S4).

In light of these findings and to further characterize the contribution of *IFT140* to disease, especially its renal and retinal aspects, we next investigated whether variants in *IFT140* occur more frequently in JATD patients than in a cohort of patients with nonciliopathy diseases. The *IFT140* sequence of the latter group was available through the UK10K WES project, comprising hypercholesterolemia (71 exomes) and severe insulin resistance (63 exomes) patients, jointly representing "nonciliopathy" exomes. We firstly established there was an equivalent *IFT140* sequence coverage between all 46 JATD exomes, and the 134 nonciliopathy exomes (Supp. Fig S5). We then compared the number of *IFT140* missense mutations unique to each patient group that were predicted to be damaging. This revealed a moderate but significant enrichment of rare (MAF < 1% in UK10K and EVS exomes) missense *IFT140* alleles in the cohort of 46 JATD patients compared with the 134 controls (odds ratio 11.72, $P = 0.0005$ with a 95% confidence interval using loci-based analysis and odds 12.45, $P = 0.0003$ with a 95% confidence interval using sample-based analysis). No statistically significant enrichment was detected when total missense changes including variants with a MAF >1% were measured (Fig. 4). Rare variants in noncoding areas of *IFT140* (3′ and 5′ UTRs, intronic and intergenic changes) or synonymous changes did not reveal any enrichment either, indicating that the enrichment in rare deleterious missense changes is not due to a generally higher number of mutations in the JATD cohort or higher number of polymorphisms due to ethnical background [Davis et al., 2011]. These findings indicate a possible role for heterozygous *IFT140* mutations as disease-modifying rather than causative alleles, but the fairly small number of samples and mutations analyzed will require further studies to confirm these findings. Also, due to low sample numbers, no analysis was performed for rare heterozygous frame-shift (one present in 46 JATD cases, zero in 134 controls), stop (zero in 46 JATD cases, zero in 134 controls) or splice site mutations (two in 46 JATD cases, zero in 134 controls).

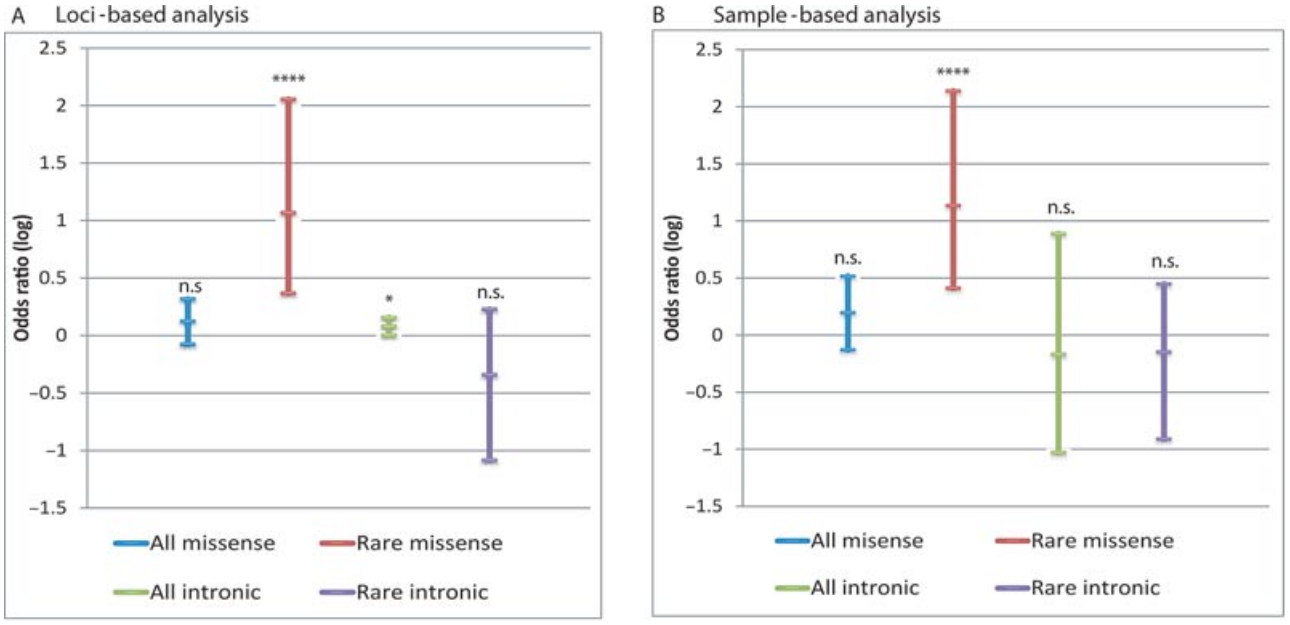

Loci-based analysis

Experiment	Cases (n = 46)	Controls (n = 134)	Fisher exact test	Original			Log		
			P-value	Odds ratio	Lower CI (95%)	Upper CI (95%)	Odds ratio	Lower CI (95%)	Upper CI (95%)
All missense	31	68	0.2008	1.33499	0.8398842	2.0799016	0.125478	-0.075780589	0.318042789
Rare missense	8	2	0.0004815	11.72487	2.334948	113.588583	1.069108	0.368277213	2.055334682
All intronic	194	474	0.03591	1.204799	1.008834	1.434451	0.0809146	0.003819711	0.156685718
Rare intronic	3	12	0.2837	0.4555475	0.08237142	1.69148432	-0.3414663	-1.084223447	0.228267976

Sample-based analysis

Experiment	Cases (n = 46)	Controls (n = 134)	Fisher exact test	Original			Log		
			P-value	Odds ratio	Lower CI (95%)	Upper CI (95%)	Odds ratio	Lower CI (95%)	Upper CI (95%)
All missense	20	44	0.2141	1.569402	0.7434396	3.2893239	0.195734	-0.12875431	0.517106641
Rare missense	8	2	0.0003247	13.63918	2.575959	137.369084	1.134788	0.410938946	2.137889002
All intronic	44	130	0.6463	0.678518	0.09352765	7.74423877	-0.168439	-1.029059978	0.888978735
Rare intronic	3	12	0.7632	0.710534	0.1228906	2.8092111	-0.148415	-0.910481335	0.448584376

Figure 4. Enrichment of *IFT140* missense variants in JATD cases. Upper panels: Graphs showing the relative enrichment of rare (MAF < 1%) coding nonsynonymous *IFT140* variants in JATD patients (n = 46) compared with n = 134 pooled nonciliopathy disease controls (hypercholesterolemia and severe insulin resistance patients). **A**: shows the analysis based on loci (variant) number, (**B**) shows the analysis based on sample number (i.e., number of individuals), with odd's ratio values plotted on a log scale. Lower panels: Enrichment statistics showing the significance values contained in (**A**) and (**B**). Both analyses revealed significant enrichment of rare nonsynonymous coding *IFT140* variants in JATD patients versus controls (**** P < 0.0005, odds ratio 11.7 for loci-based analysis and 13.6 for the sample-based analysis). All the eight rare JATD and two rare control missense mutations used in the analysis are described in Supp. Table S4. No enrichment was found for rare intronic, all intronic, or all nonsynonymous coding changes by either analysis. The loci-based analysis showed a minimal enrichment of total intronic changes in JATD patients versus controls that reaches borderline significance (odds ratio 1.2, P = 0.04) not found in the sample-based analysis. P values below 0.005 and odds ratio higher than 2 is shown in red in the tables.

A recent study has shown that IFT140 localizes to the basal bodies and ciliary axonemes in kidney tubules [Jonassen et al., 2012]. Using the same antibody published in this report, raised against mouse Ift140, we found that the protein was expressed in both basal bodies and the ciliary axoneme of the chondrogenic ATDC5 mouse cell line (Supp. Fig. S6). Although all our IFT140 patients present with cone-shaped epiphyses, narrow thorax, and typical pelvis features in case of JATD, overall the skeletal phenotype, especially the thorax phenotype, appears rather mild as there were only minor respiratory problems reported while kidney and eye phenotype presented very prominently. We therefore investigated the tissue-specific expression of *Ift140* using the lacZ-allele of a previously reported conditional *Ift140*-knockout mouse [Jonassen et al., 2012]. In agreement with the features found in the *IFT140*-deficient patients we describe here, *Ift140* gene expression levels in E15.5 embryos appeared much more prominent in the kidney and eye compared with the skeleton (Supp. Fig. S7).

Discussion

In total, we screened 66 families with JATD and MSS and identified causative *IFT140* mutations in four (6%) JATD and two MSS families, all of whom displayed early onset renal disease. Signs of retinal disease were initially reported in only a subset of patients based on patient history and fundoscopy, but were finally detected in all patients after reexamination. Notably, 17% of the JATD cohort screen had renal disease screened (11/64 patients), and 36% (four of 11) of these patients carried biallelic *IFT140* variants. From this study, we conclude that *IFT140* is a rare cause of JATD in general, but a frequent cause of JATD with renal involvement. The majority of *IFT140* patients in our study also displayed retinal deficits. We are therefore able to define for the first time a major connection in JATD between the patient's underlying genotype and the expressed clinical phenotype, indicating that *IFT140* should be prioritized for clinical diagnosis in the

proportion of JATD patients with kidney disease with and without retinal involvement.

IFT140 encodes a 1462 amino acid protein that is involved in IFT as a highly conserved core IFT-A component [Ishikawa and Marshall, 2011]. Loss-of-function mutants in *Drosophila*, trypanosomes, *C. elegans*, and mice have fewer or short cilia and defective IFT [Absalon et al., 2008; Jonassen et al., 2012; Lee et al., 2008; Qin et al., 2001). In mice, *Ift140* knockout is lethal around mid-gestation suggesting a fundamental role in embryonic development, whereas conditional knockout leads to severe and early cystic kidney disease [Jonassen et al., 2012]. Ift140 deficiency in the retina also leads to progressive retinal degeneration in mice (Gregory J. Pazour, unpublished data). Strikingly, we found all biallelic *IFT140* patients to present with renal disease in early childhood and notable retinal involvement, but they have a nonlethal thorax-related clinical course, and no polydactyly. In accordance with these findings, we found more prominent expression of *Ift140* in renal and retinal tissue in mouse embryos than in the skeleton using an *Ift140* lacZ-reporter mouse developed by G.J.P., although we found that Ift140 clearly localizes to the ciliary axoneme in murine ATDC5 chondrocyte precursor cells in immunofluorescence. These data suggest that the JATD phenotype may be substratified according to the underlying genotype.

It is possible that certain variable characteristics within the ciliopathy spectrum could not only be explained by different expression patterns but also by functional redundancy of the different IFT protein components. However, the phenotypic differences between ciliary skeletal dysplasias such as Sensenbrenner Syndrome, JATD, other SRPS forms and MSS may also indicate gene-specific effects on more than one downstream signaling pathway. IFT140 for example interacts with the calcium channel TRPV4 in *Drosophila* [Lee et al., 2008], and TRPV4 is involved in dominantly inherited skeletal dysplasias in humans [Andreucci et al., 2011]. Interestingly, TRPV4 interacts with Polycystin-2 the ion channel mutated in autosomal dominant polycystic kidney disease, and they are both thought essential for mechanosensory functions of renal cilia [Kottgen et al., 2008]. So although TRPV4 knockdown in zebrafish does not cause kidney cysts [Kottgen et al., 2008], TRPV4 protein might still be involved in ciliary functions in the kidney. *Drosophila* IFT140 mutants exhibit loss of TRPV4 localization to the cilium indicating IFT140 may target TRPV4 to the cilium [Lee et al., 2008]. *IFT140* mutations may therefore lead to failure of TRPV4 localization to the cilium, possibly affecting its kidney ciliary signaling functions.

Eight of the *IFT140* mutations we have identified in biallelic patients are novel, whereas one is a splice mutation c.2399+1G>T shared between family MSS2 and a previously reported JATD and MSS family [Perrault et al., 2012], suggesting a possible mutational hotspot or European-origin Founder effect that would therefore be diagnostically and clinically important for planning disease management. Although *IFT140* mutations are relatively rare amongst JATD patients, we also discovered putative Serbian Founder effects, involving two damaging missense mutations p.V292M and p.G522E affecting three families. Functional validation of the V292M mutation detected in three Serbian families revealed impaired localization to centrosomes to a similar extent as that described for previously reported mutations causing MSS [Perrault et al., 2012].

The mutation spectrum revealed for both JATD and MSS disorders shows that no affected individual carries two protein truncating changes, as only combinations of missense or missense plus null alleles were present in patients, rather than two null alleles together. Thus, some retention of *IFT140* activity in patients may be necessary for early embryonic survival. This observation is in agreement with observations for mutations in other genes causing phenotypes within the short rib-polydactyly spectrum [Beales et al., 2007; Dagoneau et al., 2009; Davis et al., 2011; Merrill et al., 2009; Schmidts et al., 2013]. Likewise, no significantly different clinical features could be determined between *IFT140* patients with two potentially hypomorphic missense mutations and those carrying combined missense and truncating mutations. Both JATD and MSS arose in this cohort in association with a missense and null allele (JATD1, MSS1, and MSS2). Therefore, we conclude that no connections between the nature of the mutations and the disease phenotype are yet possible for *IFT140*, although the MSS-associated mutations were all located early on at the N-terminus of IFT140 in our study, whereas the JATD-associated alleles were distributed across the protein.

We have detected a statistically significant enrichment of predicted deleterious variants in *IFT140* by WES in JATD patients, compared with non-JATD patient groups. No renal disease has been reported in four JATD patients that we identified as carrying a single deleterious *IFT140* variant alone, except for patient JATD5 who had renal deficits. JATD5 carried a early trucating mutation and could likely have a second variant allele that has missed detection in the current study. These *IFT140* single heterozygous mutations may contribute to the skeletal phenotype but when present as a heterozygous change may not be sufficient to cause kidney cysts. However, because we have looked at a only small patient number in this study, further studies with larger cohorts are required to test if this hypothesis holds true.

In summary, here we have identified mutations in *IFT140* using a combination of different sequencing approaches emphasizing the benefit of NGS in significantly improving genetic diagnostics, and in providing rapidly growing insight into genetically heterogeneous and potentially allelic diseases such as the ciliopathies. The discovery of further genetic heterogeneity underlying JATD seems likely in the future, given that approximately two thirds of all JATD patients we have analyzed do not carry mutations in coding areas of *IFT140* or in any of the previously described JATD-causing genes [Schmidts et al., 2013 and unpublished data]. *IFT140* is the first described gene causing Mainzer-Saldino Syndrome, and we find that *IFT140* mutations in JATD seem to be causal only for a specific subset of cases with severe renal and prominent retinal involvement, in the context of heterozygous mutations potentially modifying the skeletal phenotype. In future, the identification of additional *IFT140* patients within either the JATD or MSS patient group may shed further light on the reasons for the underlying clinical variability, and the reasons for the apparently milder skeletal clinical course arising from *IFT140* mutations.

Acknowledgments

The authors would like to thank the families for their cooperation and interest in the study. We thank Steve Humphries, Marta Futema, David Savage, Rob Semple, and Ines Barroso for generous permission to use their UK10K exome data and Beate Langner-Wegscheider, Department of Ophthalmology, Medical University Graz for her ophthalmological expertise. V.F., T.E., C.D., N.B., H.B., and C.B. are employees of Bioscientia, a member of Sonic Healthcare.

Disclosure statement: The authors declare no conflict of interest.

References

1000 Genome Project Consortium. 2010. A map of human genome variation from population-scale sequencing. Nature 467:1061–1073.

Absalon S, Blisnick T, Kohl L, Toutirais G, Dore G, Julkowska D, Tavenet A, Bastin P. 2008. Intraflagellar transport and functional analysis of genes required for flagellum formation in trypanosomes. Mol Biol Cell 19:929–944.

Adzhubei IA, Schmidt S, Peshkin L, Ramensky VE, Gerasimova A, Bork P, Kondrashov AS, Sunyaev SR. 2010. A method and server for predicting damaging missense mutations. Nat Methods 7:248–249.

Andreucci E, Aftimos S, Alcausin M, Haan E, Hunter W, Kannu P, Kerr B, McGillivray G, McKinlay Gardner RJ, Patricelli MG, Sillence D, Thompson E, et al. 2011. TRPV4 related skeletal dysplasias: a phenotypic spectrum highlighted byclinical, radiographic, and molecular studies in 21 new families. Orphanet J Rare Dis 6:37.

Baker K, Beales PL. 2009. Making sense of cilia in disease: the human ciliopathies. Am J Med Genet C Semin Med Genet 151C:281–295.

Beales PL, Bland E, Tobin JL, Bacchelli C, Tuysuz B, Hill J, Rix S, Pearson CG, Kai M, Hartley J, Johnson C, Irving M, et al. 2007. IFT80, which encodes a conserved intraflagellar transport protein, is mutated in Jeune asphyxiating thoracic dystrophy. Nat Genet 39:727–729.

Bredrup C, Saunier S, Oud MM, Fiskerstrand T, Hoischen A, Brackman D, Leh SM, Midtbo M, Filhol E, Bole-Feysot C, Nitschke P, Gilissen C, et al. 2012. Ciliopathies with skeletal anomalies and renal insufficiency due to mutations in the IFT-A gene WDR19. Am J Hum Genet 89:634–643.

Dagoneau N, Goulet M, Genevieve D, Sznajer Y, Martinovic J, Smithson S, Huber C, Baujat G, Flori E, Tecco L, Cavalcanti D, Delezoide AL, et al. 2009. DYNC2H1 mutations cause asphyxiating thoracic dystrophy and short rib-polydactyly syndrome, type III. Am J Hum Genet 84:706–711.

Davis EE, Zhang Q, Liu Q, Diplas BH, Davey LM, Hartley J, Stoetzel C, Szymanska K, Ramaswami G, Logan CV, Muzny DM, Young AC, et al. 2011. TTC21B contributes both causal and modifying alleles across the ciliopathy spectrum. Nat Genet 43:189–196.

DePristo MA, Banks E, Poplin R, Garimella KV, Maguire JR, Hartl C, Philippakis AA, del Angel G, Rivas MA, Hanna M, McKenna A, Fennell TJ, et al. 2011. A framework for variation discovery and genotyping using next-generation DNA sequencing data. Nat Genet 43:491–498.

Donaldson MD, Warner AA, Trompeter RS, Haycock GB, Chantler C. 1985. Familial juvenile nephronophthisis, Jeune's syndrome, and associated disorders. Arch Dis Child 60:426–434.

Ferrer-Costa C, Gelpi JL, Zamakola L, Parraga I, de lC X, Orozco M. 2005. PMUT: a web-based tool for the annotation of pathological mutations on proteins. Bioinformatics 21:3176–3178.

Frank V, Eisenberger T, Eitel C, Decker C, Bolz HJ, Bergmann C. 2012. NGS-panel targeting 150 cilia-related disease genes improves diagnostic testing for the broad spectrum of ciliopathies. Eur J Hum Genet 20 Suppl 1: C15.5.

Gherman A, Davis EE, Katsanis N. 2006. The ciliary proteome database: an integrated community resource for the genetic and functional dissection of cilia. Nat Genet 38:961–962.

Giedion A. 1979. Phalangeal cone shaped epiphysis of the hands (PhCSEH) and chronic renal disease—the conorenal syndromes. Pediatr Radiol 8:32–38.

Goetz SC, Anderson KV. 2010. The primary cilium: a signalling centre during vertebrate development. Nat Rev Genet 11:331–344.

Gonzalez-Perez A, Lopez-Bigas N. 2011. Improving the assessment of the outcome of nonsynonymous SNVs with a consensus deleteriousness score, Condel. Am J Hum Genet 88:440–449.

Huangfu D, Anderson KV. 2005. Cilia and Hedgehog responsiveness in the mouse. Proc Natl Acad Sci USA 102:11325–11330.

Ishikawa H, Marshall WF. 2011. Ciliogenesis: building the cell's antenna. Nat Rev Mol Cell Biol 12:222–234.

Jonassen JA, Sanagustin J, Baker SP, Pazour GJ. 2012. Disruption of IFT complex A causes cystic kidneys without mitotic spindle misorientation. J Am Soc Nephrol 23:641–651.

Kottgen M, Buchholz B, Garcia-Gonzalez MA, Kotsis F, Fu X, Doerken M, Boehlke C, Steffl D, Tauber R, Wegierski T, Nitschke R, Suzuki M, et al. 2008. TRPP2 and TRPV4 form a polymodal sensory channel complex. J Cell Biol 182:437–447.

Lee E, Sivan-Loukianova E, Eberl DF, Kernan MJ. 2008. An IFT-A protein is required to delimit functionally distinct zones in mechanosensory cilia. Curr Biol 18:1899–1906.

Lehman AM, Eydoux P, Doherty D, Glass IA, Chitayat D, Chung BY, Langlois S, Yong SL, Lowry RB, Hildebrandt F, Trnka P. 2010. Co-occurrence of Joubert syndrome and Jeune asphyxiating thoracic dystrophy. Am J Med Genet A 152A:1411–1419.

Li H, Durbin R. 2010. Fast and accurate long-read alignment with Burrows-Wheeler transform. Bioinformatics 26:589–595.

Li H, Handsaker B, Wysoker A, Fennell T, Ruan J, Homer N, Marth G, Abecasis G, Durbin R. 2009. The sequence alignment/map format and SAMtools. Bioinformatics 25:2078–2079.

Li D, Roberts R. 2001. WD-repeat proteins: structure characteristics, biological function, and their involvement in human diseases. Cell Mol Life Sci 58:2085–2097.

Liu X, Jian X, Boerwinkle E. 2011. dbNSFP: a lightweight database of human nonsynonymous SNPs and their functional predictions. Hum Mutat 32:894–899.

Mainzer F, Saldino RM, Ozonoff MB, Minagi H. 1970. Familial nephropathy associated with retinitis pigmentosa, cerebellar ataxia and skeletal abnormalities. Am J Med 49:556–562.

McKenna A, Hanna M, Banks E, Sivachenko A, Cibulskis K, Kernytsky A, Garimella K, Altshuler D, Gabriel S, Daly M, DePristo MA. 2010. The Genome Analysis Toolkit: a MapReduce framework for analyzing next-generation DNA sequencing data. Genome Res 20:1297–1303.

Meng EC, Pettersen EF, Couch GS, Huang CC, Ferrin TE. 2006. Tools for integrated sequence-structure analysis with UCSF Chimera. BMC Bioinform 7:339.

Merrill AE, Merriman B, Farrington-Rock C, Camacho N, Sebald ET, Funari VA, Schibler MJ, Firestein MH, Cohn ZA, Priore MA, Thompson AK, Rimoin DL, et al. 2009. Ciliary abnormalities due to defects in the retrograde transport protein DYNC2H1 in short-rib polydactyly syndrome. Am J Hum Genet 84:542–549.

Mortellaro C, Bello L, Pucci A, Lucchina AG, Migliario M. 2010. Saldino-Mainzer syndrome: nephronophthisis, retinitis pigmentosa, and cone-shaped epiphyses. J Craniofac Surg 21:1554–1556.

Nagy A, Gertsenstein M, Vintersten K, Behringer R. 2003. Manipulating The Mouse Embryo: A Laboratory Manual (3rd edn). Cold Spring Harbor, NY: Cold Spring Harbor Laboratory Press.

Nigg EA, Raff JW. 2009. Centrioles, centrosomes, and cilia in health and disease. Cell 139:663–678.

Oberklaid F, Danks DM, Mayne V, Campbell P. 1977. Asphyxiating thoracic dysplasia. Clinical, radiological, and pathological information on 10 patients. Arch Dis Child 52:758–765.

Ocbina PJ, Anderson KV. 2008. Intraflagellar transport, cilia, and mammalian Hedgehog signaling: analysis in mouse embryonic fibroblasts. Dev Dyn 237:2030–2038.

Perrault I, Saunier S, Hanein S, Filhol E, Bizet AA, Collins F, Salih MA, Gerber S, Delphin N, Bigot K, Orssaud C, Silva E, et al. 2012. Mainzer-Saldino syndrome is a ciliopathy caused by IFT140 mutations. Am J Hum Genet 90:864–870.

Qin H, Rosenbaum JL, Barr MM. 2001. An autosomal recessive polycystic kidney disease gene homolog is involved in intraflagellar transport in *C. elegans* ciliated sensory neurons. Curr Biol 11:457–461.

Rix S, Calmont A, Scambler PJ, Beales PL. 2011. An Ift80 mouse model of short rib polydactyly syndromes shows defects in hedgehog signalling without loss or malformation of cilia. Hum Mol Genet 20:1306–1314.

Roy A, Kucukural A, Zhang Y. 2010. I-TASSER: a unified platform for automated protein structure and function prediction. Nat Prot 5:725–738.

Schmidts M, Arts HH, Bongers EMHF, Yap Z, Oud MM, Antony D, Duijkers L, Emes RD, Stalker J, Yntema J-BL, Plagnol V, Hoischen A, et al. 2013. Exome sequencing identifies DYNC2H1 mutations as a common cause of asphyxiating thoracic dystrophy (Jeune syndrome) without major polydactyly, renal or retinal involvement. J Med Genet. Published Online First: 1 March 2013 doi:10.1136/jmedgenet-2012-101284

Schwarz JM, Rodelsperger C, Schuelke M, Seelow D. 2010. MutationTaster evaluates disease-causing potential of sequence alterations. Nat Methods 7:575–576.

Thiel C, Kessler K, Giessl A, Dimmler A, Shalev SA, von der HS, Zenker M, Zahnleiter D, Stoss H, Beinder E, Abou JR, Ekici AB, et al. 2011. NEK1 mutations cause short-rib polydactyly syndrome type majewski. Am J Hum Genet 88:106–114.

Yang Z, Lasker K, Schneidman-Duhovny D, Webb B, Huang CC, Pettersen EF, Goddard TD, Meng EC, Sali A, Ferrin TE. 2011. UCSF Chimera, MODELLER, and IMP: an integrated modeling system. J Struct Biol 179:269–278.